AIP | The Journal of Chemical Physics

Different structures give similar vibrational spectra: The case of OH− in aqueous solution

Pavlin D. Mitev, Philippe A. Bopp, Jasmina Petreska, Kaline Coutinho, Hans Ågren et al.

Citation: J. Chem. Phys. **138**, 064503 (2013); doi: 10.1063/1.4775589

View online: http://dx.doi.org/10.1063/1.4775589

View Table of Contents: http://jcp.aip.org/resource/1/JCPSA6/v138/i6

Published by the American Institute of Physics.

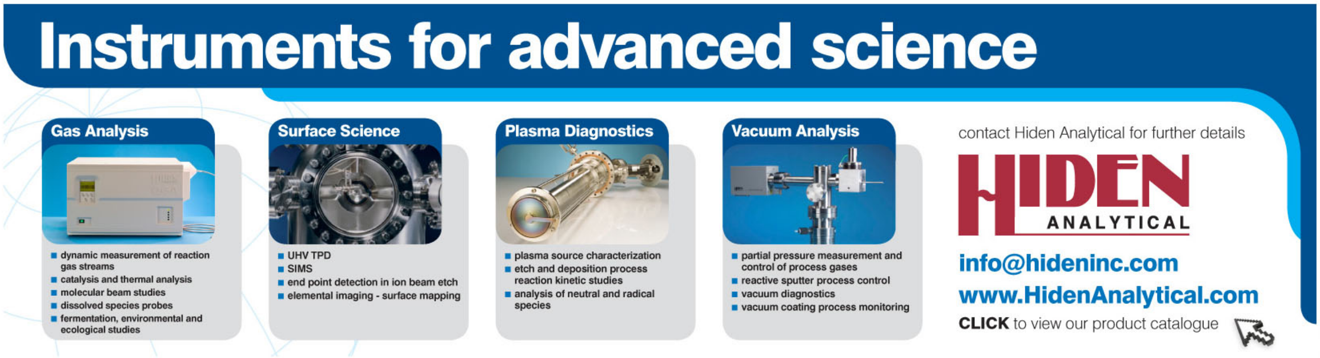

THE JOURNAL OF CHEMICAL PHYSICS **138**, 064503 (2013)

Different structures give similar vibrational spectra: The case of OH^- in aqueous solution

Pavlin D. Mitev,[1,2] Philippe A. Bopp,[3] Jasmina Petreska,[4] Kaline Coutinho,[5] Hans Ågren,[2] Ljupco Pejov,[4,a)] and Kersti Hermansson[1,2,a)]
[1]*Department of Chemistry - Ångström, Uppsala University, Box 538, SE-751 21 Uppsala, Sweden*
[2]*Department of Theoretical Chemistry, School of Biotechnology, Royal Institute of Technology, SE-106 91 Stockholm, Sweden*
[3]*Department of Chemistry, 351 Cours de la Libération Bât. A12, Université de Bordeaux, FR-33405 Talence CEDEX, France*
[4]*Institute of Chemistry, Faculty of Science, "Sts. Cyril and Methodius University," P.O. Box 162, 1000 Skopje, Republic of Macedonia*
[5]*Instituto de Física, Universidade de São Paulo, CP 66318, 05315-970 São Paulo, SP, Brazil*

(Received 25 February 2012; accepted 23 December 2012; published online 11 February 2013)

We have calculated the anharmonic OH^-(aq) vibrational spectrum in aqueous solution with a "classical Monte Carlo simulation + QM/MM + vibrational" sequential approach. A new interaction model was used in the Monte Carlo simulations: a modified version of the charged-ring hydroxide-water model from the literature. This spectrum is compared with experiment and with a spectrum based on CPMD-generated structures, and the hydration structures and H-bonding for the two models are compared. We find that: (i) the solvent-induced frequency shift as well as the absolute OH^- frequency are in good agreement with experiment using the two models; (ii) the Raman and IR bands are very similar, in agreement with experiment; (iii) the hydration structure and H-bonding around the ion are very different with the two ion-water interaction models (charged-ring and CPMD); (iv) a cancellation effect between different regions of the hydration shell makes the total spectra similar for the two interaction models, although their hydration structures are different; (v) the net OH^- frequency shift is a blueshift of about $+80$ cm^{-1} with respect to frequency of the gas-phase ion. © *2013 American Institute of Physics*. [http://dx.doi.org/10.1063/1.4775589]

I. INTRODUCTION

Different experimental and theoretical techniques have been used to unravel the hydration features of the hydroxide ion. Structural information has been reported from neutron diffraction experiments combined with an empirical potential structure refinement approach in Ref. 1. A combined X-ray diffraction and simulation study was presented in Ref. 2. X-ray absorption spectroscopic measurements and core-level electron spectroscopy have been used to explore the nature of the OH^- hydration in solution.[3,4] These and other studies were mentioned in the review by Marx *et al.* in Ref. 5.

Intramolecular stretching vibrational spectra often give valuable information about the local structure around the vibrating oscillator. Vibrational spectroscopic studies (Raman or IR) from experiments and calculations for OH^- in water were recently reviewed by Hermansson *et al.*[6] (cf. Table I in that paper). The experimental Raman study by Corridoni *et al.*[7] showed that the $\nu(OH^-)$ frequency upshift ("blueshift") in aqueous solution compared to the gas-phase lies in the range +50 to +80 cm^{-1}, depending on the concentration.

We discuss here what structural features of the hydration shell lie behind this upshift and whether the solvent-induced $\Delta\nu(OH^-)$ is indeed a sensitive probe of the ion's hydration structure and the H-bonding to (and from?) it. We use a sequential "simulation + QM/MM + vibrational" method to calculate the anharmonic vibrational OH spectrum. The interaction model in the simulation stems from the charged-ring (CR) OH^- model of Ufimtsev *et al.*[8] We will find that this approach leads to vibrational spectra and spectral shifts in agreement with experiment. Moreover, by comparing with similar calculations based on CPMD simulations in Ref. 6, we will find that the solvent-induced $\Delta\nu(OH^-)$ may not be a sensitive probe of the local structure around the ion.

More precisely, we showed in Ref. 6 that a sequential "CPMD+QM/MM+vibrational" computational method also managed to reproduce the experimentally observed solvent-induced OH^- frequency blueshift, and we discussed the origin of the shift in terms of the electric field effects that give rise to the OH frequency shift. Now we will compare the ion hydration structures generated by the classical FF and DFT (density functional theory) models of the two simulations, and investigate why the CPMD and the force field model give similar vibrational spectra, although the hydration structures and ion-water H-bonding are found to differ in some important respects, in both the oxygen (O*) and hydrogen (H*) hemispheres of the ion.

In summary, IR and Raman measurements of an aqueous hydroxide solution yield a broad spectral band in the OH stretching region. This band has contributions from the bulk water molecules, the water molecules around the cations

---

[a)] Electronic addresses: ljupcop@iunona.pmf.ukim.edu.mkl and kersti@kemi.uu.se.

and the anions, the hydroxides ions, and the small number of proton transfer entities that are long-lived enough to give a signature on the measured spectra. The goal of the present study is, in keeping with our previous work,[6] to pinpoint the contributions from the hydroxide ions themselves to the OH spectrum, i.e., hydroxide ions which are clearly identifiable as such and, for example, not involved in any proton transfer processes.

We first review the computational procedures and report the calculated vibrational band. We then decompose this vibrational band into region-resolved spectra, i.e., contributions ascribed to different regions of the hydration shell, and proceed to a detailed comparison of the hydration shells obtained from the previous CPMD and the present MC simulations. Both are found to be *a priori* equally reasonable.

II. COMPUTATIONAL PROCEDURE

Monte Carlo simulations were performed for a 0.7 *m* $OH^-(aq)$ solution at 300 K. Configurations were extracted from the simulation and used in quantum-mechanical (QM) calculations of the (anharmonic) OH^- intramolecular potential energy curves $V_{OH}(r_{OH})$. The one-dimensional vibrational Schrödinger equation was solved for each of these curves assuming the reduced mass of $^{16}O/^{1}H$, yielding $0 \rightarrow 1$ transition energies, which were then binned in a histogram. The average frequency of these histograms, as well as fitted Gaussian and Lorenzian functions, were analyzed and the frequency shifts were calculated with respect to the isolated gas-phase monomer frequency. Proton transfer is not considered in the present study. The MC simulation was performed with the DICE Monte Carlo suite of codes[9] and all quantum-chemical calculations were performed with the GAUSSIAN 09 program.[10] As for the vibrational frequency calculations, we use our own set of programs.

We label the hydroxide ion's atoms O* and H* and the water atoms O_w and H_w.

A. System and simulation procedure

The Monte Carlo (MC) simulation was performed using cubic periodic boundary conditions in all three directions. The simulation box contained one (rigid) hydroxide anion plus 83 (rigid) water molecules of the SPC[11] type. This corresponds to the highest dilution under which the hydroxide ion's OH stretching band in the experimental Raman spectra in Ref. 7 could still be clearly resolved. The simulation was performed in the isothermal-isobaric (*NpT*) ensemble at $T = 298$ K, $p = 1$ atm (average box length 13.43 Å, average density 1.04 g/cm^3, which is slightly larger than the density of liquid SPC water at 300 K and ambient pressure (0.99 g/cm^3)). A thermalization phase of 2.52×10^7 MC steps was followed by an averaging (simulation) phase of 1.26×10^8 MC steps.

B. The intermolecular potentials

For the water molecule, we used the SPC model[11] potential. For the hydroxide ion, a modified version, called here "mod-CR," of the original "charged-ring" (CR) model of Ufimtsev *et al.*[8] was used. In both the mod-CR and the original CR model of Ref. 8, the O charge site is replaced by a charge density distribution over a hard mass-less ring rigidly attached to the oxygen atom (Fig. 1). The ring mimics the electron density distribution of the oxygen lone-pair region of a hydroxide ion. The CR charge was split into 20 discrete point charges distributed uniformly on the ring, following the procedure in Ref. 8.

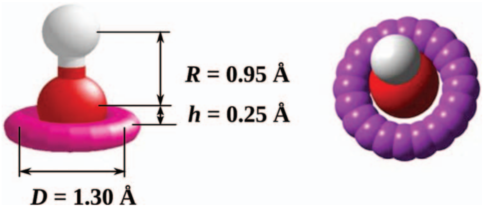

FIG. 1. Interaction sites for the electrostatic part of the charged-ring model for the OH^- ion: Charges of 0.07420 *e* and −0.05377 *e* (see Ref. 8) are placed on the H site and on each of the 20 sites on a massless ring perpendicular to the O–H bond and intersecting it 0.25 Å beyond the O atom.

We added to the electrostatic interactions the Lennard-Jones 12-6 site-site interaction terms proposed in Ref. 8. We have, however, omitted the additional repulsive exponential term that was also used in Ref. 8 and kept only the Lennard-Jones *r*-12 term to describe the repulsion. This was done because we wanted a less repulsive variant of the potential of Ufimtsev *et al.*[8]; the original potential gives a coordination number of 4.1 water molecules out to the first minimum in the O*–H_w radial distribution function (rdf) and 3.9 for R(O*–O_w) $<$ 3.3 Å (calculated by us from the curves given in Fig. 4(a) of Ref. 8). The CPMD simulations in the literature give about 5.2 water O_w atoms within R(O*–O_w) $<$ 3.4 Å (Zhu and Tuckerman[12] and Megyes *et al.*[2]), in agreement with the neutron diffraction results of McLain *et al.*[1] The new model yields coordination numbers closer to the experimental one than the original CR model (see later).

Long-range corrections were applied for the calculation of the interaction energy. The Lennard-Jones energy was estimated assuming a uniform density distribution in the liquid (i.e., $g(r) \approx 1$) while the electrostatic contribution was estimated by the reaction field method involving the dipolar interactions.

C. Selection of MC configurations

Configurations were selected from the simulation for different purposes: (i) for a structural analysis, (ii) for a pair interaction energy (PIE or Δ*E*) analysis to explore the strength of the water-ion interaction in the first hydration shell, and (iii) for the OH^- frequency calculations. In the first two cases, 1500 configurations were selected. In the latter case, many quantum-mechanical single point calculations need to be performed for each potential energy curve, which limits the number of configurations that can be allowed for. One hundred OH^- oscillators and their environments were selected from the MC run for subsequent vibrational calculations.

One hundred is a relatively small number of structures to represent the accessible configurational space. Coutinho *et al.* (see Ref. 13, and references therein) proposed a method to diagnose the correlation between configurations, which we have used here. This analysis gives a "correlation length" (τ) of 435 MC-steps. According to this measure, MC configurations separated by 1305 steps ($3 \cdot \tau$) are less than 10% correlated. The 100 configurations that we selected from our 1.26×10^8 step run, correspond to one configuration every 15 000 steps, and have thus a negligible (3.5×10^{-8}%) correlation.

D. QM calculations and the determination of the frequency distributions and shifts

A cluster of water molecules was selected around the hydroxide ion for each MC "snapshot" selected for the frequency calculation. For each snapshot, electronic structure calculations were performed to generate the anharmonic intramolecular OH^- potential energy curve for subsequent frequency calculations.

Thus, each cluster was composed of a central OH^- ion *plus* all water molecules residing within an $R(O_w \cdots O^*)$ distance of less than 3.5 Å in the O* hemisphere *plus* all water molecules residing within an $R(O_w \cdots H^*)$ distance of less than 4.5 Å in the H* hemisphere. These limits are liberal enough to include the first hydration shell, and more, as will become obvious from the structural analysis in the results part of the paper. In fact, in total 10−16 water molecules were included in the quantum-mechanical (QM) clusters for the various snapshots: 4−6 in the O* hemisphere and 5−11 in the H* hemisphere. The geometry of the cluster was kept frozen at the MC configuration, except for the O–H distance of the ion, which was varied.

To take care of long-range interactions, each QM cluster was point-charge-embedded by water molecules out to a distance of half the average box length during the simulation, and the water atoms were given the SPC charges. The QM methods used were Hartree-Fock (HF; as reference), second-order Möller-Plesset perturbation theory (MP2), and DFT of the B3LYP[14,15] type. The standard Pople-style 6-31++G(*d*,*p*) basis set was used because we have previously found that it reproduces the experimental shape of the potential energy curve for the gas-phase hydroxide ion very well at the B3LYP level,[6] and also appears to describe the solvent induced perturbations of this curve well in aqueous solution.[6] All energies were corrected for the basis-set superposition error (BSSE).[16]

The OH^- ion's stretching vibration is thus assumed to be decoupled from those of the surrounding water molecules. We use the discrete variable representation of Ref. 17 to calculate the vibrational states and the energy difference between the two lowest energy levels was converted to (anharmonic) frequency values, using the masses $m(O) = 15.994915$ amu and $m(H) = 1.007825$ amu. The frequencies were collected in histograms and asymmetric variants of Gaussian and Lorentz line shapes according to Stancik and Brauns[18] were fitted to the histograms. Harmonic frequencies were calculated from the curvatures of the potential energy curves at the $r_e(OH)$ values.

Analogue calculations for the isolated gas-phase hydroxide ion yielded the values 3865, 3551, and 3651 cm^{-1} for the fundamental anharmonic O–H stretching frequency at the HF, B3LYP, and MP2 levels of theory, respectively. The experimental anharmonic gas-phase value is 3556 cm^{-1},[19] which shows that the B3LYP/6-31++G(*d*,*p*) level of theory yields excellent agreement of the absolute frequency with the experimental value. These frequencies are listed in Table I and will be discussed below.

Raman intensities are proportional to the square of the derivative of the molecular polarizability with respect to the vibrational coordinate ("the transition polarizability"). For water, this quantity has been shown to display only a small variation in quite diverse environments.[20] We have not performed a similar investigation for the hydroxide ion, but assume that the variation is also not large here. We will thus compare our resulting vibrational density-of-states (DOS) histogram for OH^-(aq) with the experimentally observed Raman results.

To compute the IR band, the generated DOS histograms need to be converted to IR intensity-weighted histograms by means of the transition dipole moment function $|d\vec{\mu}/dr|^2$. The transition dipole moment function was calculated for each oscillator at r_e from the expression: $[(d\vec{\mu}/dr)_{re}]^2 = [(d\mu_x/dr)_{re}]^2 + [(d\mu_y/dr)_{re}]^2 + [(d\mu_z/dr)_{re}]^2$. Each of the derivatives on the right-hand side of this expression was computed by a fourth-order polynomial interpolation of the corresponding $\mu_i(r)$ function and subsequent differentiation at r_e. Newton's interpolation formulas were used for both the fourth-order polynomial interpolation and the numerical differentiation.

E. Exclusion of proton transfer processes

As mentioned in the introduction, in this paper we focus on hydroxide ions which are clearly identifiable as such and not involved in proton transfer processes. In general, in an MD simulation, such a separation can be achieved in a fairly straightforward manner by excluding any snapshots which are deemed as "proton transfer cases," e.g., by using suitable distance criteria. This is what we did in the analysis of the CPMD simulations in Ref. 6. In the present case, the underlying MD simulations consist of rigid molecules so no proton transfers can take place.

To which extent could this simplification lead to an erroneous physical picture? The review by Marx *et al.*[5] discusses structural diffusion and the *presolvation* concept, which means that "*in any proton transfer reaction* [...] *the proton-receiving species, i.e., the acceptor site, must first have a solvation pattern that corresponds to the species into which it will be transformed as a result of the reaction.*" If this picture holds, the exclusion of snapshots at or close to proton transfer in the CPMD simulation in Ref. 6 would not bias the calculated OH^- spectrum, since such "preparation structures" would still be included, as long as OH^- is still an OH^-. Likewise, using an MD model with rigid molecules should in principle also include those structures.

Roberts *et al.*,[21] on the other hand, rather emphasize the structural diffusion occurring after the proton transfer

TABLE I. Calculated frequencies and frequency shifts (in cm^{-1}) with respect to the isolated ion for the 100 OH^-(aq) anharmonic oscillators with potential energy surfaces computed with three different QM methods. Experimental Raman frequencies are also listed. No scaling factors were used.

	HF		B3LYP		MP2		Raman experiment[a]	
	ν	$\Delta\nu$	ν	$\Delta\nu$	ν	$\Delta\nu$	ν	$\Delta\nu$
OH^-(g)[b]	3865	0	3551	0	3651	0	3556	0
OH^-(aq): average	4042	+177	3653	+102	3725	+74		
OH^-(aq): Peak max[c]	4016	+151	3641	+90	3710	+59	3633	+77
OH^-(aq): Peak max[d]	4017	+152	3637	+86	3707	+56		

[a] The gas-phase value is taken from Ref. 19 and the aqueous solution value is from Ref. 7 (see text for more details).

[b] Only one frequency value for the isolated oscillator, i.e., no average.

[c] Position of the peak maximum of a Gaussian function fitted to the frequency histograms (see text).

[d] Position of the peak maximum of a Lorenzian function fitted to the frequency histograms (see text).

("*the transport of a proton requires not only the solvation of the new OH^- ion, but also that of the newly formed water molecule*"). Moreover, they conclude that the structural diffusion following the transfer is slow (~3 ps). Excluding the snapshots where the proton is in transit in a CPMD simulation, as discussed above, would both give "clean OH^-" ions (as we want) and capture many of the odd coordinations that may follow the transfer (according to Ref. 21) and affect the OH^- spectrum. However, if we totally disallow proton transfers to happen, as in our present MD simulations, such odd configurations would be missing. The effect of missing this subset is probably small, but it should be mentioned.

III. RESULTS AND DISCUSSION

A. Vibrational OH^- stretching band

We constructed here frequency histograms from the computed anharmonic OH stretching frequencies for the 100 selected oscillators (Fig. 2). In Table I these and experimental anharmonic frequencies are given together with the gas-to-liquid shifts. The computed frequency values in the table were obtained in three different (average, Gaussian peak max, Lorentzian peak max) ways from frequency histograms like the ones shown in the figure, and the uncertainty was estimated to be about ±2 cm^{-1}.

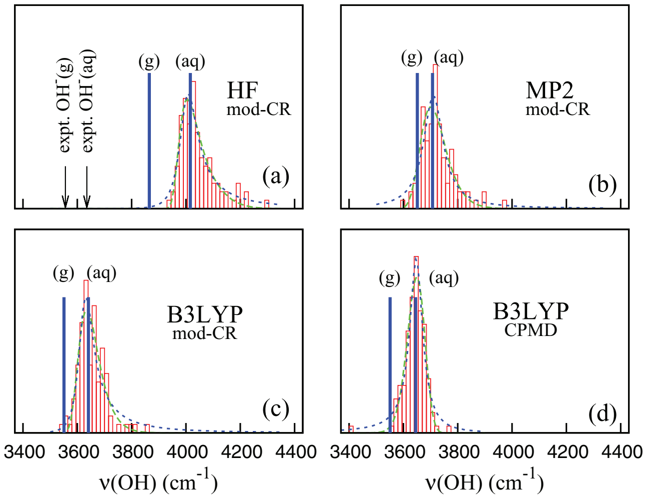

FIG. 2. Vibrational bands of anharmonic frequencies from our multi-stage procedure, based on structures from the mod-CR MC simulation (this work) in (a)–(c), and structures from the CPMD simulation in (d) (Ref. 6). The QM method listed (HF, MP2, B3LYP) denotes the method used in the calculation of the solvent-affected OH^- potential energy curves. The corresponding calculated gas phase frequencies are also given. The experimental values are indicated in (a).

The "mod-CR" curves in Fig. 2 show that the gas-to-liquid frequency shifts resulting from the "MC + QM/MM + vibrational" procedure using the B3LYP and MP2 method for the QM/MM step, are close to the experimental value. The HF level of theory, on the other hand, gives significantly poorer agreement with the experimental observations. Both the MP2 and B3LYP methods show a blueshift, and with the B3LYP method the absolute frequencies are in good agreement with experiment.

We also tested the inclusion of polarizability for the bulk solvent molecules by embedding the QM supermolecules in a polarizable continuum by means of the Onsager variant of the self-consistent reaction field method (SCRF). The QM cluster was then placed in a spherical cavity with a radius which was 0.5 Å larger than that computed from the approximate molecular volume (defined as the volume inside a contour of 0.001 electrons/bohr^3 electronic density) calculated by Monte Carlo integration of the electronic density corresponding to the particular level of theory used. The average gas-to-liquid frequency shifts for the 100 OH oscillators were found to differ by less than 10 cm^{-1} from those presented in Table I. Thus, at least within the simplest SCRF methodology, accounting for polarization of the solvent outside the first hydration shell appears to have little influence on the OH^- frequency.

We also explored the effect of IR-intensity weighting of the OH^- frequencies using the calculated instantaneous dipole moment derivatives, the squares of which are plotted in Fig. 3 against the instantaneous frequencies. There are no systematic variations of the dipole moment derivative in the relatively small frequency span created by the aqueous OH^- ion, and the IR and Raman bands are thus very similar, as experiments predict them to be.

The full widths at half heights were calculated for the Gaussian probability distribution functions fitted to the various histograms. The results are 94, 89, and 111 cm^{-1}, respectively, at the Hartree-Fock, B3LYP, and MP2 levels for the Raman bands; to be compared with the experimentally measured half-widths of 70-85 cm^{-1} (Ref. 7). We do not know of any convenient way to correct for the motional narrowing effect present in the experiments. Moreover, the neglect of

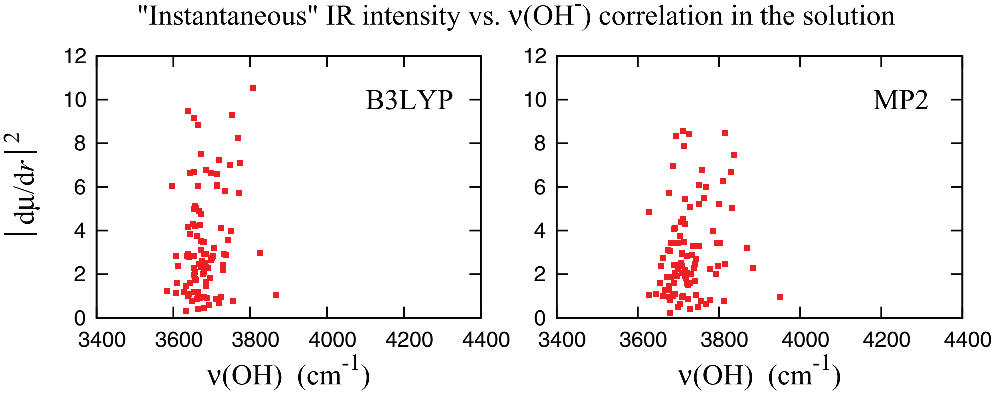

FIG. 3. Dipole moment derivatives of the OH^- ion calculated quantum-mecanically for the OH^- ion for the 100 selected MC snapshots, and plotted as a function of anharmonic vibrational frequency. B3LYP/ 6-31++G(*d*,*p*) (left) and MP2/6-31++G(*d*,*p*) (right) calculations.

rotational-vibrational coupling may have an influence on the linewidth. The good agreement observed between the computed bandwidths and the experimental data may therefore be somewhat fortuitous.

The *average* solvent-induced change of the intramolecular OH bond was calculated and found to be less than 0.01 Å at all three QM levels, and it is a contraction, which was expected, given that the average OH stretching vibrational frequency is known to be closely related to the average intramolecular OH bond distance. However, such a correlation is not necessarily expected to hold for the various *instantaneous* local environments represented by our snapshots from the solution structure, where only the intramolecular distance of the probed oscillator has been optimized (frozen environment). Figure 4 displays the calculated 100 OH^- frequencies vs. the corresponding equilibrium bond lengths (r_e), i.e., the minima of the 100 QM_{elec}-calculated potential energy curves. Overall, the ν(OH) vs. r_e dependence is actually seen to be quite linear, however with an appreciable spread around the correlation line. The spread in the present case is larger than in our studies of OH frequencies for water next to cations in aqueous solutions;[22] this is understandable given the large structuring effect of the cations. The slopes obtained here are about half of the values we obtained earlier for HDO water around cations in aqueous ionic solutions.

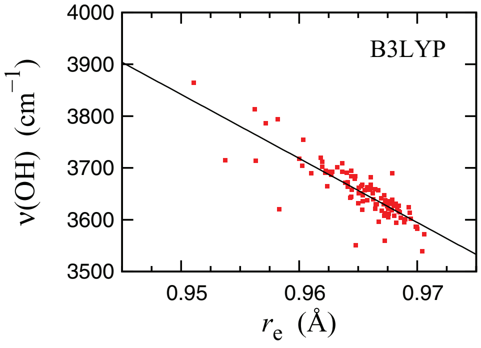

FIG. 4. Correlation between the resulting instantaneous OH^- vibrational frequency and the position of the minimum of the effective vibrational potential for the 100 snapshots from the mod-CR MC simulation, investigated with B3LYP/6-31++G(*d*,*p*) calculations.

In summary: Based on the hydration structures generated with the mod-CR hydroxide-water intermolecular model and the B3LYP approximation for the intramolecular potential curves we calculate a reasonable vibrational band profile compared to experiment, and the absolute position of the spectrum is also very good. This was also true when the underlying structures were generated from the CPMD simulation in Ref. 6. The band positions are thus in good agreement between the two methods. The band shapes are slightly different without it being possible to say which one would be more realistic. Before we proceed with the analysis of these bands, we investigate the hydration shell structure with the mod-CR model and then come back to the vibrational bands and the comparison between the two models.

B. Hydration shell structure: Water$\cdots$O* radial distributions

The red solid curve in Fig. 5(a) shows the $O^*\cdots O_w$ rdf calculated from the mod-CR Monte Carlo simulation. It bears much resemblance to the experimental curve by McLain *et al.* (Fig. 4 in Ref. 1) based on neutron diffraction measurements combined with empirical potential structure refinement. We note that in both cases, the first peak maximum of g_{O*Ow} is high (~6 in experiment, ~7 in our calculations) and narrow, the second peak has a maximum of about 1.3-1.5 at ~4.3 Å, and the minimum between the first and second peaks goes down to about 0.6. The location of the first peak occurs at a shorter distance in the experiment-based curve, namely, at ~2.2 Å (which may be a bit too short in our opinion) compared to the mod-CR value of ~2.5 Å.

The $O^*\cdots O_w$ first-shell coordination number reported in the experimental study in Ref. 1 is 5.2. The CPMD simulation study of Zhu and Tuckerman[12] and that of Megyes *et al.*[2] gave coordination numbers between 5.0 and 5.2 out to the first-shell $O^*\cdots O_w$ minimum at 3.4 Å (there is a misprint in Table VI of Ref. 2, where it is stated that the minimum occurs at 3.1 Å with the coordination number 4.92, but the values should be 3.4 Å and 5.2 water molecules[23]). Taking these results together, it appears likely that more than 4 water molecules reside within the first $R(O^*\cdots O_w) < 3.4$ Å sphere of the hydroxide ion. Ufimtsev's original CR model

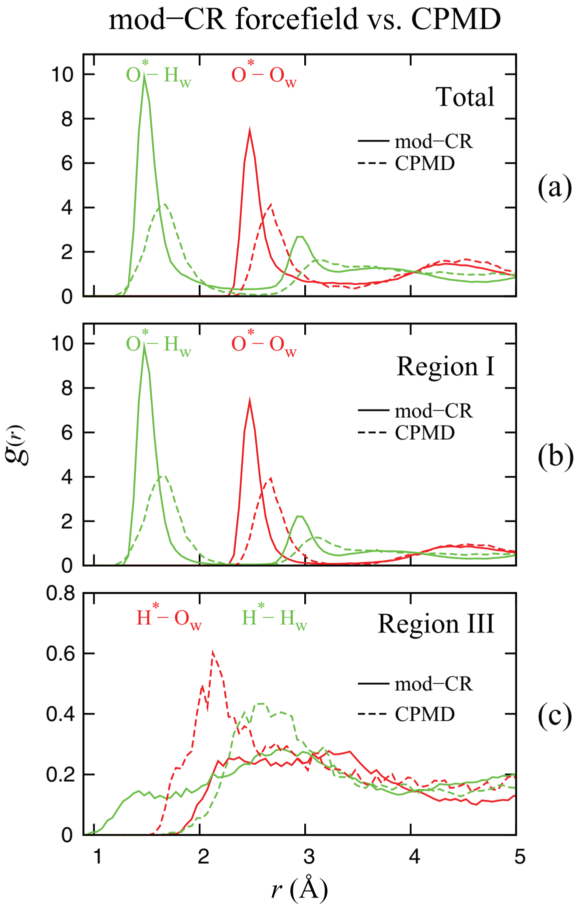

FIG. 5. Selected distribution functions for the mod-CR (solid lines) and CPMD (dashed line) models. (a) Total O*–H_w (green) and O*–O_w (red) distribution functions, i.e., Regions I, II, and III together. (b) O*–H_w (green) and O*–O_w (red) functions in Region I, (c) H*–O_w (green) and H*–H_w functions in Region III.

gives a coordination number of 3.9 water molecules surrounding the hydroxide ion (calculated by us from Fig. 4(a) in Ref. 8). Our exclusion of the repulsive terms added by Ufimtsev *et al.*[8] (see Sec. II B) leads to a higher coordination number: integration over the first peak in the O*$\cdots$$O_w$ rdf curve up to the first minimum (at 3.4 Å) gives a hydration number of 6.6.

The average hydration structure around the hydroxide ion in the MC simulation is illustrated in the dotplot in Fig. 6. The red circle around the O* atom marks the 3.4 Å cutoff just discussed. The positions of the centers-of-mass of the water molecules are shown as dots. The dot is green if at least one of the water molecule's H_w atoms is closer to the ion than the O_w atom is. "Closer to the ion" means closer to the hydroxide O* atom in the O* hemisphere and closer to H* in the H* hemisphere. The dot is red if the water O_w is closer than a H_w to the ion. This plot looks quite different from the corresponding one obtained from the CPMD simulations (Fig. 7 in Ref. 6).

C. Water molecules residing in the H* hemisphere (Regions II and III)

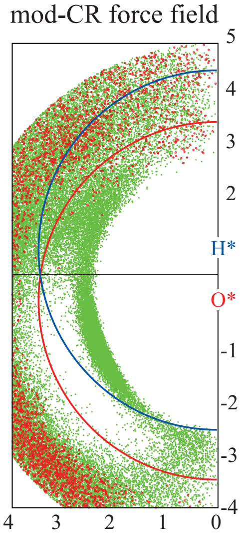

FIG. 6. Representation of the positions and orientations of the water molecules relative to the ion for 3000 well separated configurations from the mod-CR MC simulation. Each dot represents the position of the center-of-mass of a water molecule. The dot is red/green if the water molecule has an O_w/H_w atom oriented closest to the ion (clostest to the ion means closest to the O* atom in the O* hemisphere and closest to the H* atom in the H* hemisphere). The circles delimit spheres with a radius of 3.4 Å around O* and H*.

The space around the OH^- ion was then subdivided for the structural analysis into angular domains. Figure 7 illustrates this partition of the space around the ion: Region I is the hemisphere out to large distances on the O* side, as illustrated in the figure, while the H* hemisphere is divided into two parts. In some of the discussion below we will additionally introduce a distance cut-off.

We have analyzed the water structure in the different regions around the hydroxide ion. Figs. 5(b) and 5(c) show distribution functions, analogous to rdfs, but normalized differently, in the Regions I and III. The functions are normalized so that the sum of the three regions is set to 1 at large distance,

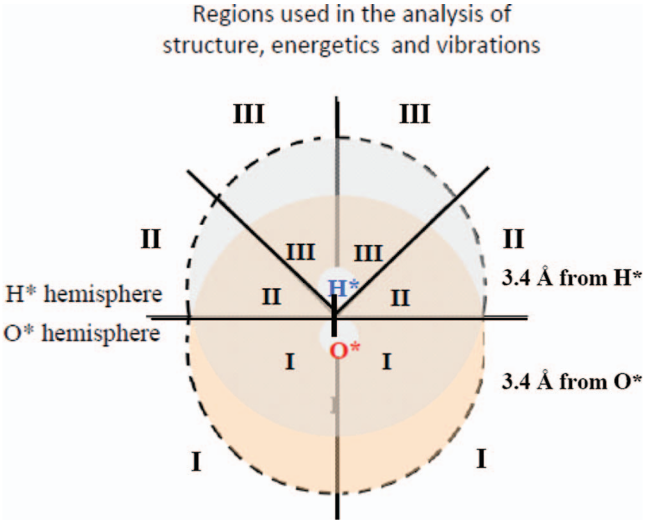

FIG. 7. Definition of the angular regions. Region I is the O* hemisphere, Regions II and III subdivide the H* hemisphere. Region III is a cone with an opening angle of 90°. In some cases we will particularly consider only those water molecules that lie within the dumbell region defined in the figure, i.e., the union of two spheres with radii 3.4 Å, centered around O* and H*, respectively.

TABLE II. Average coordination (hydration) numbers in the dumbell-shaped volume resulting from the union of the two spheres of radii 3.4 Å from O* and H*, respectively (Fig. 7). The total coordination numbers and the contributions from Regions I, II, and III within this dumbell are given; the regions are also defined in Fig. 7. The minima in the water-ion B3LYP pair interaction energy distributions for the mod-CR (Fig. 8(a)) and the CPMD (Fig. 8(b)) solutions fall at about −20 and −15 kcal/mol, respectively; these numbers are used as cutoffs in the table, as indicated.

	Coordination number			
	Total	Region I	Region II	Region III
	mod-CR MC structures			
$R(O^*-O_w) < 3.4$ Å	6.6	4.8	1.5	0.3
The whole dumbell	8.1	4.8	2.2	1.1
$\Delta E^{B3LYP} < -20$ kcal/mol	4.7	4.4	0.3	0.0
$\Delta E^{B3LYP} < -5$ kcal/mol	7.0	4.7	1.9	0.4
$\Delta E^{B3LYP} > -5$ kcal/mol	1.1	0.1	0.3	0.7
	CPMD structures			
$R(O^*-O_w) < 3.4$ Å	5.2	3.9	0.6	0.6
The whole dumbell	6.5	3.9	1.2	1.4
$\Delta E^{B3LYP} < -15$ kcal/mol	3.9	3.6	0.3	0.0
$\Delta E^{B3LYP} < -5$ kcal/mol	4.2	3.7	0.5	0.1
$\Delta E^{B3LYP} > -5$ kcal/mol	2.3	0.2	0.6	1.3

i.e., the amplitude of each function represents the contribution of each region to the total rdf. It is seen that while the distributions in Region I are typically sharper, and at somewhat shorter distances, for mod-CR than for the CPMD model, the inverse in true in Region III, where the CPMD distributions are more peaked, although they are both much more featureless in Region III than in Region I.

The number of water molecules that (on average) reside in the O* and H* hemispheres, or the different regions, are listed in Table II. We note first that for both the mod-CR and CPMD models, there is a significant contribution to the first-shell $O^* \cdots O_w$ rdf peak from water molecules residing in the H* hemisphere (i.e., the contributions from Regions II and III listed on the lines labelled "$R(O^*-O_w) < 3.4$ Å" in Table II). The dotplot in Fig. 6 suggests that a cutoff radius of 3.4 Å from the O* atom (the red circle around the O* atom) may be too small for the mod-CR solution and may exclude some of the first-shell waters on the H* side (in particular in Region III, where the first and second shells seem to merge). We therefore see it fit to use a slightly larger volume to define the first hydration shell, namely, the volume formed by the union of two spheres of radii 3.4 Å, one centered on the O* atom, the other on the H* atom, as also illustrated in Fig. 6. The results are given on the lines labelled "the whole dumbell" in Table II and refers to all water molecules residing within the dumbell. With this definition, the mod-CR model gives 8.1 waters molecules in the first hydration shell: 60% in Region I and 30% in Region II and 10% in Region III. With this definition we possibly include on the H* side some fraction of water molecules which would more appropriately be described as second shell or bulk. On the other hand, as our energy analysis below will show, the majority of these 8.1 water molecules bind appreciably to the anion.

D. H-bonding (Regions I, II, and III)

The definition of H-bonds in simulations has been the object of long-standing discussions in the literature: in addition to geometric criteria and vibrational frequency shifts, interaction energies provide useful insight. Figure 8(a) displays the solute-solvent pair-interaction energy histograms for the 1500 MC snapshots, calculated with the B3LYP interaction model (BSSE-corrected interaction energies using the 6-31++G(*d*,*p*) basis sets). The energies binned are $\Delta E = E(OH^- \cdot H_2O) - E(OH^-) - E(H_2O)$, where all species have the geometry taken from the MC snapshot. A negative interaction energy means binding.

The peak at large negative values in Fig. 8(a), i.e., for $\Delta E < -20$ kcal/mol, might be interpreted as the hydrogen-bond peak, and we shall discuss if this is a reasonable interpretation. Using this H-bond energy criterion gives 4.7 H-bonded water molecules around the ion within the dumbell volume (Table II). These essentially constitute the population of strongly H-bonded water molecules in the vicinity of the plane of the charged ring, most of which lie in Region I, and some in Region II, as is implied in the dotplot in Fig. 6 and seen more clearly from the region-specific curves in Fig. 8(a) and the numbers in Table II. These water molecules form quite

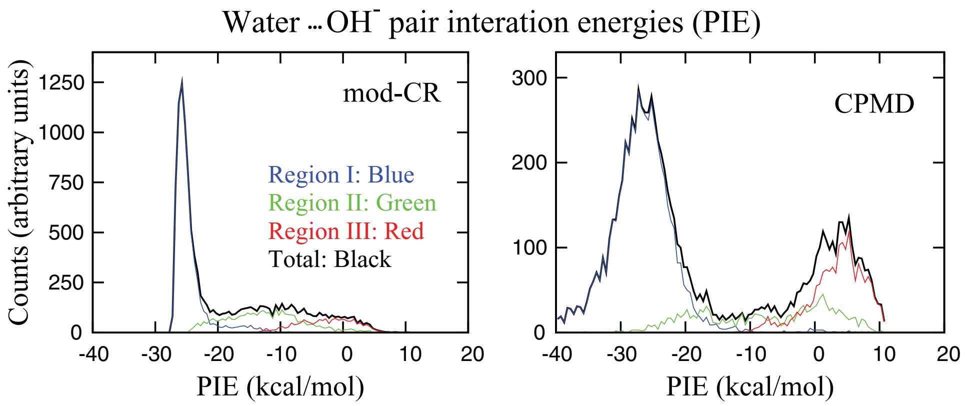

FIG. 8. Histogram of the water-OH⁻ pair interaction energies (PIE) computed quantum-mechanically (BSSE-corrected at the B3LYP/ 6-31++G(*d*,*p*) level) for all ion-water pairs from 1500 well separated snapshots taken from (a) the MC simulations with the mod-CR model and (b) the CPMD simulation. For each snapshots, all water molecules within the dumbell region shown in Fig. 5 were considered. Results for each of Regions I, II, and III, as well as the total, are shown.

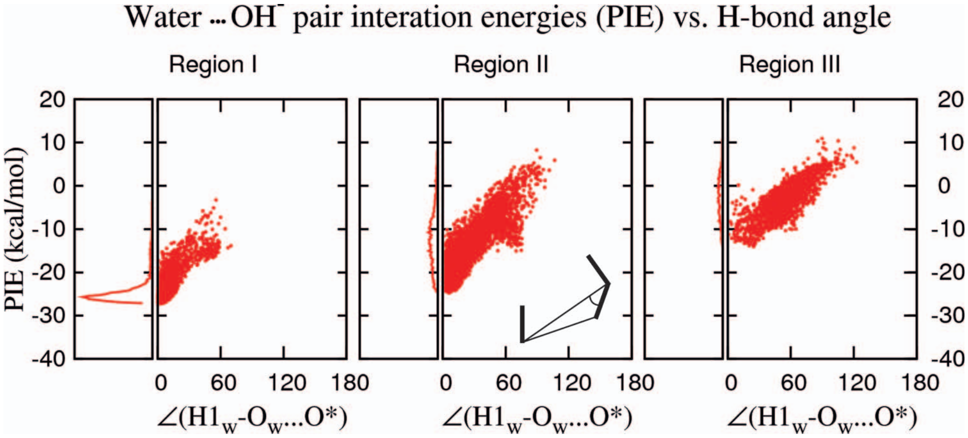

FIG. 9. The interaction energies from Fig. 8(a), computed as a function of the $H1_w$–O_w–O* angle (see inset in the plot for Region II: $H1_w$ is the water H atom closest to the ion, meaning closest to O* in Region I and closest to H* in Regions II and III.). The small frames on the left-hand side in each panel show the same curves as in Fig. 8(a).

straight H-bonds with H-bond angles typically less than 25°, as can be seen from the energy-angle correlation plots in Fig. 9. The H-bond angle is here defined as the $H1_w - O_w \cdots O^*$ angle, where $H1_w$ is the water H atom closest to the ion (see the inset in the middle panel of Fig. 9).

There are also some moderately strongly bound first-shell water molecules in Regions II and III. For the mod-CR model, 2.3 of the water molecules within the *first hydration dumbell* belong to the population of water molecules which interact with the ion with energies in the range $-20 < \Delta E < -5$ kcal/mol (Table II). Virtually all of these water molecules point a hydrogen atom (rather than the O_w atom) towards the hydroxide ion, as shown by their $H1_w - O_{w.} \cdots O^*$ angle being <90° and often, less than 45°, in Fig. 9. Thus they *donate H-bonds* to the negative ion. The remaining 1.1 water molecules within the dumbell have ΔE values above −5 kcal/mol. Among these is a small fraction of water molecules that reside "above" the H* atom and are oriented in such a way that their O_w atoms reside closer to H* than the H_w atoms do. They all have *repulsive pair interaction energies* and are thus not really bound to the ion itself, although favorable interactions with the rest of the water framework keep them in place.

A similar situation occurs in the CPMD-generated solution, where there are actually many more such repulsive molecules (cf. for example the dotplot in Ref. 6 where Region III is much more "red" than in the mod-CR dotplot). Although such $O^* - H^* \cdots O_w$ arrangements fulfill standard geometric H-bond criteria, the positive interaction energy is not in keeping with conventional energetic H-bond definitions. We concluded in Ref. 6 that the hydroxide ion in the CPMD solution appears not to be an H-bond donor and we conclude here that, even without the additional repulsion in the original Ufimtsev potential, the hydroxide ion is not an H-bond donor in the mod-CR solution.

In summary, the mod-CR potential leads to a higher number of *first-shell* water molecules around OH⁻ than predicted by the CPMD results. It gives 6.6 water molecules within $R(O^*–O_w) < 3.4$ Å, or 8.1 within the dumbell region, but the number of H-*bonded* water molecules is 4.7 when strict H-bond energy criteria are used (guided by Fig. 8). This means that almost 1 more water molecule is strongly H-bonded than for the CPMD solution; this extra water molecule, present in many snapshots, is a water molecule that resides "below" the O* atom close to the exterior of the O*H* axis (cf. the green region in the dotplot in Fig. 6). In the mod-CR solution, another ∼2 water molecules per ion donate weaker H-bonds to the ion with an ion-water pair interaction energy in the range between −5 and −20 kcal/mol, mostly located in Regions II and III. Such water molecules are almost missing in the CPMD solution (here it is more appropriate to use the energy limits −5 and −15 kcal/mol in the analysis; see Fig. 8(b)). Instead, in the H* hemisphere, the CPMD trajectory has considerable more snapshots which contain ∼1 water molecule oriented with O_w towards H*; these have ion-water interaction energies that are repulsive or close to zero.

IV. REGION-RESOLVED SPECTRA FOR THE TWO MODELS

We have found that the present MC simulation with the mod-CR model and subsequent B3LYP calculations yield a distribution of OH⁻ frequencies, and an average solvent-induced OH⁻ frequency shift, in good agreement with experiment, see Fig. 2. This was also found to be true for the CPMD-generated structures in Ref. 6. However, the structures generated by the two simulations reveal significant differences, which can up to now not be resolved by experimental or other means.

Figure 10 shows the decomposition of the bands according to the location of the neighboring molecules. While the water neighbors in Region I cause a larger OH⁻ frequency upshift with the mod-CR structures than with the CPMD structures, the opposite is true for Region III. No marked difference is found in Region II. The mutual cancellation of these shifts leads to the overall agreement of the frequency distributions with each other (and with experiment, see however the argument about linewidth made above).

The implication of this analysis, i.e., that two more or less equally plausible hydration structures can be constructed

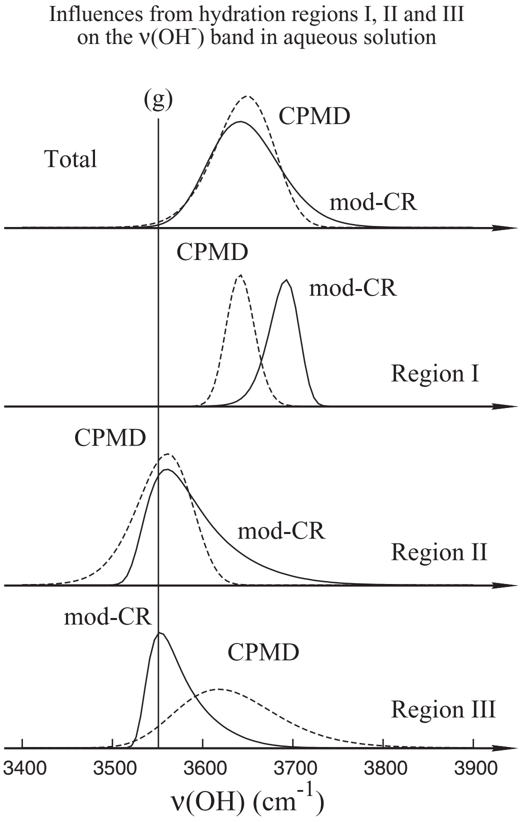

FIG. 10. Analysis of the total vibrational OH^-(aq) spectrum in terms of shifts caused by the various angular regions around the ion. The upper panel shows the Gaussian fits to the bands when all water molecules are taken into account, the three lower panels show the bands when only the water molecules in the respective regions are included in the vibrational calculations. The B3LYP method was used for the potential energy curves in all cases here.

that yield the same band for the OH^- vibration, is that this vibration may not be a sufficiently sensitive probe of the surrounding structure. The shift of the band with respect to the gas phase and its shape result from electric fields generated mostly by the first hydration shell of the ion. They can either add up or cancel each other, making any direct link between structure and vibrational band a tenuous one at best.

V. SUMMARY

The solvent-induced blueshift of the intramolecular vibration of the OH^- ion in aqueous solution has been revisited using the charged-ring hydroxide-water interaction model. We obtain quite similar bands here and in the CPMD study in Ref. 6, in reasonable agreement with Raman data, even though the linewidth may not be directly compared due to the omission of the experimental motional narrowing.

We used here the SPC model for water and a modified charged-ring description of the electron distribution around the hydroxide O atom. With this modification the OH^- ion accepts 4.7 hydrogen bonds on average (using an energy criterion of $\Delta E < -20$ kcal/mol for the ion-water pair interaction at the B3LYP level). On average, another couple of water molecules reside in the first hydration shell defined as all waters out to the first minimum in the O^*–O_w rdf curve (∼3.4 Å), giving a coordination number of 6.6. These numbers differ from the previously reported one from CPMD studies; however, also for the CPMD solution the number of strongly bound H-bonded water molecules is smaller than the coordination number (3.9 vs. 5.2).

In order not to miss any nearest-neighbor water molecules that may bind favourably to the hydroxide ion on the H* side, we defined a hydration dumbell. This analysis showed that for the mod-CR model almost all of the ∼8 water molecules in the dumbell bind to the ion via their H_w atom(s), i.e., also on the H* side, and have an attractive interaction energy with the ion. In the CPMD solution, on the other hand, while having about 2 water molecules in the H* hemisphere vs. 3 for the mod-CR model, they are predominanly non-bonded or repulsive, and often oriented with O_w, and not H_w, closest to H* (see Ref. 6).

The comparison of this and the previous simulations thus demonstrates that even though there are clear differences in the ion's hydration structures between the two models, the overall solvent-induced frequency shifts, the absolute frequencies and band shapes are in agreement with experiment. We find that this is the result of a cancellation of the effects from neighbors in different regions around the ion. The vibrational spectra and solvent-induced frequency shifts may therefore not be sensitive enough to distinguish between different hydration structures around the OH^- ion in water.

ACKNOWLEDGMENTS

The authors acknowledge the support of The Swedish Research Council (VR). Lj.P. acknowledges the financial support of the Swedish Institute (post-doctoral research grant). P.A.B. thanks the Wenner-Gren foundation (Sweden) for a grant and the Ångström Laboratory for its hospitality. Computer time was provided by the Uppsala Multidisciplinary Center for Advanced Computational Science (UPPMAX) at Uppsala University and the Swedish National Infrastructure for Computing (SNIC). This work was performed within the framework of the MATTER Consortium (supported by the Knut and Alice Wallenberg Foundation, KAW) and the eSSENCE programme (a strategic research program in e-science supported by the Swedish Government).

[1] S. McLain, S. Imberti, A. Soper, A. Botti, F. Bruni, and M. Ricci, Phys. Rev. B **74**, 094201 (2006).
[2] T. Megyes, S. Bálint, T. Grósz, T. Radnai, I. Bakó, and P. Sipos, J. Chem. Phys. **128**, 044501 (2008).
[3] C. D. Cappa, J. D. Smith, B. M. Messer, R. C. Cohen, and R. J. Saykally, J. Phys. Chem. A **111**, 4776–4785 (2007).
[4] E. F. Aziz, N. Ottosson, M. Faubel, I. V. Hertel, and B. Winter, Nature (London) **455**, 89–91 (2008).
[5] D. Marx, A. Chandra, and M. E. Tuckerman, Chem. Rev. **110**, 2174 (2010).
[6] K. Hermansson, P. A. Bopp, D. Spångberg, L. Pejov, I. Bakó, and P. D. Mitev, Chem. Phys. Lett. **514**, 1–15 (2011).
[7] T. Corridoni, A. Sodo, F. Bruni, M. A. Ricci, and M. Nardone, Chem. Phys. **336**, 183–187 (2007).
[8] I. S. Ufimtsev, A. G. Kalinichev, T. J. Martinez, and R. J. Kirkpatrick, Chem. Phys. Lett. **442**, 128–133 (2007).
[9] K. Canuto and S. Coutinho, in *DICE: A Monte Carlo Program for Molecular Liquid Simulation, University of São Paulo* (1997).
[10] M. J. Frisch, G. W. Trucks, H. B. Schlegel *et al.*, GAUSSIAN 09, Revision A.1, Gaussian, Inc., Wallingford, CT, 2009.

[11] H. J. C. Berendsen, J. P. M. Postma, W. F. Van Gunsteren, and J. Hermans, in *Intermolecular Forces*, edited by B. Pullman (Reidel, 1981), pp. 331–342.
[12] Z. Zhu and M. E. Tuckerman, J. Phys. Chem. B **106**, 8009–8018 (2002).
[13] K. Coutinho, S. Canuto, and M. C. Zerner, J. Chem. Phys. **112**, 9874 (2000).
[14] A. D. Becke, J. Chem. Phys. **98**, 5648–5652 (1993).
[15] C. Lee, W. Yang, and R. G. Parr, Phys. Rev. B **37**, 785 (1988).
[16] S. F. Boys and F. Bernardi, Mol. Phys. **19**, 553–566 (1970).
[17] J. C. Light, I. P. Hamilton, and J. V. Lill, J. Chem. Phys. **82**, 1400 (1985).
[18] A. L. Stancik and E. B. Brauns, Vib. Spectrosc. **47**, 66–69 (2008).
[19] J. C. Owrutsky, N. H. Rosenbaum, L. M. Tack, and R. J. Saykally, J. Chem. Phys. **83**, 5338 (1985).
[20] S. A. Corcelli and J. L. Skinner, J. Phys. Chem. A **109**, 6154–6165 (2005).
[21] S. T. Roberts, K. Ramasesha, P. B. Petersen, A. Mandal, and A. Tokmakoff, J. Phys. Chem. A **115**, 3957–3971 (2011).
[22] L. Pejov, D. Spångberg, and K. Hermansson, J. Phys. Chem. A **109**, 5144–5152 (2005).
[23] I. Bakó (Budapest), private communication (2012).